# Heavy-ion Coulomb excitation and photon decay of the giant dipole resonance in $^{208}$Pb

J. R. Beene, F. E. Bertrand, D. J. Horen, R. L. Auble, B. L. Burks,
J. Gomez del Campo, M. L. Halbert, and R. O. Sayer
*Oak Ridge National Laboratory, Oak Ridge, Tennessee 37831*

W. Mittig and Y. Schutz
*Grand Accelerateur National d'Ions Lourds, 14021 Caen CEDEX, France*

J. Barrette,* N. Alamanos, F. Auger, B. Fernandez, and A. Gillibert
*Département de Physique Nucléaire/Basse Energie, Centre d'Etudes Nucléaires de Saclay, 91191 Gif-sur-Yvette CEDEX, France*

B. Haas and J. P. Vivien
*Centre de Recherches Nucléaires, 67037 Strasbourg CEDEX, France*
(Received 16 June 1989)

The excitation and electromagnetic decay of the giant resonance region (8–15 MeV) in $^{208}$Pb have been measured with the $^{208}$Pb($^{17}$O,$^{17}$O′) reaction at 84 MeV/nucleon. The study of coincidences between scattered $^{17}$O ions and photon decays to the $^{208}$Pb ground state, including angular correlations, serves to isolate the isovector giant dipole resonance and enable us to investigate the mechanisms of its excitation and decay in detail. The angular correlations and yields are accounted for quantitatively by a pure Coulomb excitation model of the reaction process. The distribution in energy of the ground-state photon decay cross section is well described by an approximate application of the multistep theory of nuclear reactions. The photon coincidence measurements enable us to extract the differential cross sections for the 10.6-MeV giant quadrupole and 13.9-MeV monopole resonances with low uncertainty. An analysis of the Coulomb-nuclear interference for the 10.6-MeV excitation indicates that the ratio of neutron to proton matrix elements, $M_n/M_p$, is $1.7\pm0.4$, consistent with a predominantly isoscalar character for the giant quadrupole resonance.

## I. INTRODUCTION

Inelastic scattering of hadrons has played a major role in the accumulation of information on the properties of isoscalar giant resonances over the past decade, but has made almost no contribution to our understanding of isovector electric giant resonances.[1,2] This is because of the relative weakness of the isovector part of the nucleon-nucleus interaction, which leads to small excitation cross sections for isovector states.[2] This condition no longer holds for heavy-ion scattering at bombarding energies sufficiently high that Coulomb excitation, which is indifferent to isospin character, can play a major role in the excitation of high-lying states.[2,3]

Although the angular distributions of the cross sections for excitation of nuclear states via heavy-ion inelastic scattering are not strongly characteristic of the angular momentum transfer, photon decay data can be extremely sensitive to the multipolarity of the excited state. In Fig. 1, we show the ground-state gamma width ($\Gamma_{\gamma_0}$) expected for a sharp state exhausting 100% of the relevant isoscalar (IS) or isovector (IV) energy-weighted sum rule (EWSR) as a function of multipolarity and energy, relative to that for $E1$ photons. It is clear from Fig. 1 that single-photon decay back to the ground state of an even-even nucleus from an excitation energy region that contained equal percentages of the respective EWSR would be dominated by $E1$ radiation, therefore by the isovector giant dipole resonance (IVGDR). Ground-state gamma decay can yield data on the electromagnetic strength of resonances, and provides simple, well-defined conditions under which one can investigate the multistep theory of nuclear reactions in terms of which giant resonance decay is conventionally discussed.

Figure 2 shows cross sections calculated for excitation of the IVGDR and isoscalar giant quadrupole resonance (ISGQR) in the $^{208}$Pb($^{17}$O,$^{17}$O′) reaction for incident $^{17}$O energies of 22, 50, and 84 MeV/nucleon. The cross sections shown are those at the peak, generally just inside the grazing angle, of the calculated angular distribution at the various energies. At ~20 MeV/nucleon, the cross section for excitation of the ISGQR is more than an order of magnitude larger than that of the IVGDR. However, at 84 MeV/nucleon, Coulomb excitation plays a much larger role: The cross section for the IVGDR has increased by a factor of ~400 and is larger by a factor of 2–3 than that of the ISGQR. The calculations shown in Fig. 3, based upon the methods of Satchler,[2] show that near the peak of the differential cross section at 2.7°, the contribution of nuclear excitation to the IVGDR cross section from 84 MeV/nucleon inelastic scattering of $^{17}$O from $^{208}$Pb is less than 1 part in 1000.

 

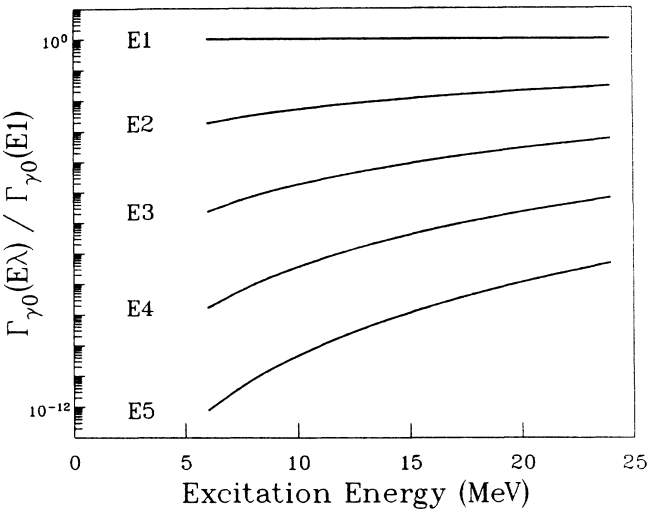


FIG. 1. Ground-state gamma widths of hypothetical sharp states fully exhausting the appropriate isovector or isoscalar energy weighted sum rule on $^{208}$Pb as a function of the excitation energy of the state, relative to the $E1$ width. The curves are based on standard expressions for the sum rules and gamma decay widths given, e.g., in Refs. 2 and 4.

Figures 1 and 2 show that at 84 MeV/nucleon the ground-state photon spectrum measured in coincidence with $^{17}$O ions that excite the giant resonance (GR) region should be dominated by $E1$ radiation. As will be shown later, this is true even at excitation energies near the peak of the giant quadrupole resonance (GQR). At 22 MeV/nucleon, the same considerations indicate that observation of photons from the GQR may be possible and we have discussed such measurements elsewhere.[4] In the

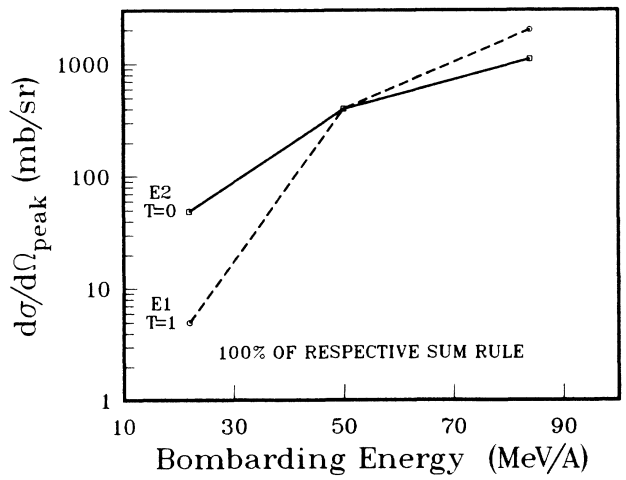


FIG. 2. The peak differential cross section for inelastic scattering of $^{17}$O from $^{208}$Pb to the resonance states indicated as a function of beam energy. These calculations were carried out using standard collective model DWBA procedures (see, e.g., Refs. 2 and 30), with the code PTOLEMY (Ref. 22).

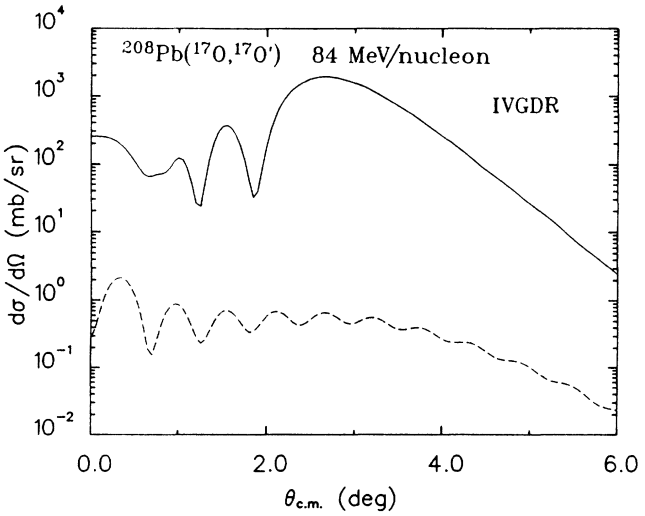


FIG. 3. DWBA calculation of IVGDR excitation by 84-MeV/nucleon $^{17}$O ions for Coulomb excitation only (solid line) and nuclear excitation only (dashed line) assuming 100% of the classical EWSR.

10–25 MeV region of excitation energy, higher multipolarities ($L > 2$) are extremely unlikely to contribute to the ground-state photon decay (Fig. 1).

In this paper we report $^{208}$Pb($^{17}$O,$^{17}$O'$\gamma$) coincidence measurements of the photon decay of the giant resonance region (9–20 MeV of excitation) made with 84 MeV/nucleon $^{17}$O ions. We verify that the ground-state photon coincidence data are dominated by the IVGDR. Thus by investigating the giant resonances in coincidence with photon decay to the $^{208}$Pb ground state, we are able to isolate the IVGDR and test its excitation mechanism in detail without recourse to a multipole peak decomposition of the GR region or any assumptions concerning underlying background. We show that the photon decay coincidence data for the IVGDR can be very accurately described by calculations of the excitation process done with the distorted-wave Born approximation (DWBA) using $E1$ strength distributions obtained from photonuclear cross sections. Therefore, we can subtract the IVGDR contribution from the GR region, leaving a much simpler spectrum from which we are able to extract accurate differential cross sections for the most important remaining peaks, the 10.6-MeV GQR and 13.9-MeV isoscalar giant monopole resonance (ISGMR). This clean isolation of the GQR cross section is particularly important. It enables us to extract the relative contributions of electromagnetic and nuclear excitation to the 10.6-MeV excitation from Coulomb-nuclear interference effects, and consequently deduce the ratio of neutron to proton matrix elements for the GQR (i.e., its isospin character). Furthermore, we can make direct comparison of the GQR strength distribution obtained in these measurements with that obtained from $(e,e'n)$ measurements. Our results also demonstrate that measurements of the photon decay following medium-energy heavy-ion Coulomb excitation of the IVGDR can provide a means for detailed nuclear studies of the dipole resonance.

## II. EXPERIMENT

The 1.43-GeV $^{17}O$ beam (84 MeV/nucleon) was provided by the Grand Accélérateur National d'Ions Lourds (GANIL) cyclotron facility. The scattered $^{17}O$ ions were detected and identified in the Spectrometer Perde Energie GANIL (SPEG) in which the momentum and scattering angle were obtained by reconstruction of the trajectories in the focal plane of the spectrometer. The overall energy resolution was $\approx 800$ keV. For measurements of the inelastic spectra, a movable absorber was inserted near the focal plane to prevent elastically scattered particles from entering the detector system. Elastic data were taken in a separate run. The $\sim 62$ mrad horizontal acceptance of the spectrometer allowed data to be acquired simultaneously over the range $1.5° \leq \theta_{c.m.} \leq 5.0°$. The vertical acceptance was 13 mrad for the elastic scattering measurements and 45 mrad for the inelastic data. The in-plane angular resolution is better than 0.2°; however, at the more forward angles the effective angular resolution is determined by the vertical acceptance of the spectrometer. The angular accuracy is estimated to be 0.05°. The absolute normalization of the cross sections was obtained from the target thickness and the integrated beam current measured in a Faraday cup. The error on the normalization is estimated to be $\pm 10\%$.

Figure 4 shows a $^{208}Pb(^{17}O,^{17}O')$ spectrum from the GANIL measurements (solid line) at 84 MeV/nucleon and a spectrum from the same reaction using 22-MeV/nucleon $^{17}O$ ions.[5] The lower energy spectrum is normalized to the 84 MeV/nucleon data at 40 MeV of excitation energy. The resonance peak ($\sim 11$ MeV) in the 22 MeV/nucleon data rises over a factor of 2 above the nuclear continuum, but even this impressive peak/continuum ratio is dwarfed by the nearly ten to one ratio observed in the 84-MeV/nucleon spectrum. It is also apparent from Fig. 4 that the excitation energy of the centroid of the giant resonance peak is higher in the GANIL data than in the lower-energy data. As we discuss in the following, and as can be inferred from Fig. 2, this is because Coulomb excitation of the IVGDR provides the largest single contribution to the GR region at the higher bombarding energy, whereas the quadrupole resonance is the stronger excitation at the lower bombarding energy.

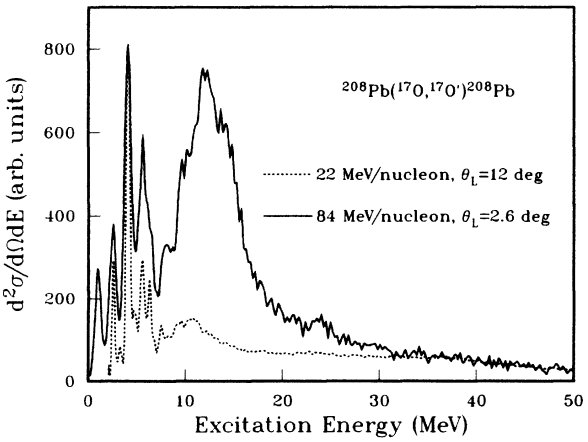


FIG. 4. Spectra from inelastic scattering of 84 and 22 (Ref. 5) MeV/nucleon $^{17}O$ from $^{208}Pb$. The two spectra are normalized in the unstructured continuum near 40 MeV.

Results from analysis of the singles spectra from 84-MeV/nucleon $^{17}O$ scattering along with more details of the spectrograph have been reported in a separate paper.[6] In that work a decomposition of the resonance peak into six peaks was made, yielding results consistent with earlier light-ion inelastic scattering data.[7] Encouraged by the excellent agreement between the measured and calculated shapes of the IVGDR, we have performed a more accurate decomposition of the singles spectra; this is shown in Sec. III B.

Gamma rays in coincidence with inelastically scattered $^{17}O$ ions were detected in four close-packed scintillator clusters, each consisting of seven hexagonal $BaF_2$ crystals of diameter 8.66-cm (face to face) and 14-cm deep. These crystals are elements of the Strasbourg Chateau de Cristal and have been described elsewhere.[8] The detectors were positioned 20 cm from the $^{208}Pb$ target, at laboratory angles $(\theta,\phi)$ of (95°,0°), (70°,180°), (134°,180°), and (90°,270°), where the angles are spherical polar coordinates defined in the conventional way with respect to a Cartesian coordinate system with the $z$ axis along the beam direction and the $y$ axis perpendicular to the reaction plane (up). In this system the scattered $^{17}O$ ions were detected with $\theta \approx 1.5°$–5° and $\phi = 0° \pm 2.6°$.

For each of the 28 gamma detectors, pulse heights and times relative to the cyclotron rf were stored along with the data from SPEG. Neutrons were identified and separated from gamma rays off line by time of flight using pulse-height (energy) dependent time gates. The photon time resolution at fixed pulse height was less than 800 ps for pulse heights corresponding to 2 MeV or more. Since pulse-shape identification of charged particles in the $BaF_2$ was not employed, the target was surrounded by an aluminum absorber that had a path length close to 3.6 cm for all photon observation angles. This thickness of aluminum corresponds to the range of $\sim 100$-MeV protons.

For study of ground-state photon decay of the giant resonance region, each of the detector clusters was treated as a single detector by digitally summing the individual pulse heights to produce a total pulse height, subject to the condition that the central detector recorded the largest single pulse. Energy and efficiency calibrations were made using radioactive sources (up to $E_\gamma = 4.43$ MeV) and on-line data for the 2.613, 4.085, and 5.512-MeV states in $^{208}Pb$, which decay by emission of a single photon to the ground state. These results were extrapolated to higher energy using simulations based on the code GEANT.[9]

## III. RESULTS AND DISCUSSION

### A. Ground-state photon decay: Isolation of the IVGDR

Figure 5 shows a spectrum of inelastically scattered $^{17}O$ ions, gated by the condition that a photon was observed in one (and only one) of the four detector clusters with energy equal, within experimental resolution, to the

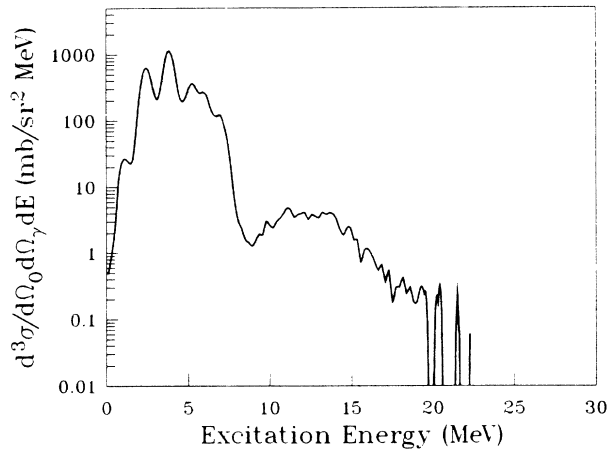


FIG. 5. Inelastic spectrum in coincidence with gamma rays to the ground state. The $^{17}$O angles are $\theta=2.0°$–$3.5°$ in this case, the gamma detector angles are given in the text.

corresponding excitation energy determined from the kinetic energy of the scattered $^{17}$O ion. Therefore, the data shown on Fig. 5 give the distribution of ground-state decays in $^{208}$Pb.

In the low-excitation-energy region, peaks are resolved for ground-state decay from 2.61-MeV, $3^-$, and 4.08-MeV, $2^+$, states, and from a group of states, probably $1^-$, located between 5 and 7 MeV. These states are strongly excited in the singles spectrum (Fig. 4). The spectrum of ground-state decays (Fig. 5) falls rapidly in intensity at the neutron separation energy ($\sim$7.4 MeV) but shows a distinct localization of strength in the excitation energy region of the IVGDR and the 10.6-MeV GQR.

Figure 6 shows the angular correlation of all ground-state photon radiation for the excitation energy interval 9–25 MeV and fixed angle of detection of the inelastically scattered $^{17}$O (2–3°) compared with the prediction for pure Coulomb excitation of the IVGDR and both Coulomb and nuclear excitation of the GQR calculated with the code ECIS.[10] Photon detector angles are shown with respect to the direction of the recoiling $^{208}$Pb nucleus. Heavy curves are calculations for $E1$ deexcitation, while the light curves are for $E2$. The solid data points and the solid curves lie in the reaction plane ($\phi=0°$ and 180°). The open point and dashed curves refer to the $\phi=270°$ half plane. One sees from Fig. 6 that, as expected, the photon coincidences are dominated by $E1$ decay from the IVGDR.

Figure 7 shows the ground-state photon-$^{17}$O angular correlation for fixed gamma angles of $\theta_\gamma=90°$ and $\phi_\gamma=270°$ and variable $^{17}$O emission angle, expressed as absolute cross sections. These cross sections can be expressed as[2]

$$\frac{d^2\sigma}{d\Omega\, d\Omega_\gamma}=\frac{1}{4\pi}\frac{d\sigma}{d\Omega}W(\theta_\gamma\phi_\gamma)R_{\gamma_0}\,, \tag{1}$$

where $d\sigma/d\Omega$ is the inelastic differential cross section, $W(\theta_\gamma\phi_\gamma)$ is the photon distribution function (which is a function of the $^{17}$O′ angle), and $R_{\gamma_0}$ is a constant that gives the total ground-state photon branching ratio. The solid line in Fig. 7 is a fit to the data with $d\sigma/d\Omega$ and $W$ obtained from a DWBA calculation, again assuming only Coulomb excitation of the IVGDR. Since the IVGDR is broad ($\Gamma\sim4$ MeV) and since the excitation probability for constant strength declines exponentially with increasing excitation energy, the calculation was carried out as a

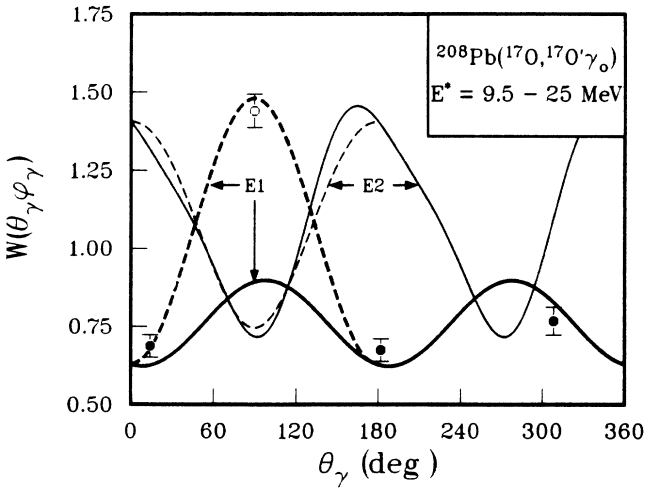


FIG. 6. Angular correlation for the $^{208}$Pb($^{17}$O,$^{17}$O′$\gamma_0$) reaction at 84 MeV/nucleon for fixed $^{17}$O′ angle ($\theta=2°$–$3°$) and varying $\gamma_0$ angle. The lines are from theoretical calculations. Solid data points and the solid curves lie in the reaction plane ($\phi=0°$ and 180°). (For convenience, the $\phi=180°$ half plane is labeled by $\theta+180°$.) The open circle and dashed lines refer to the $\phi=270°$ half plane. Heavy curves are for $E1$ deexcitation, light curves are for $E2$.

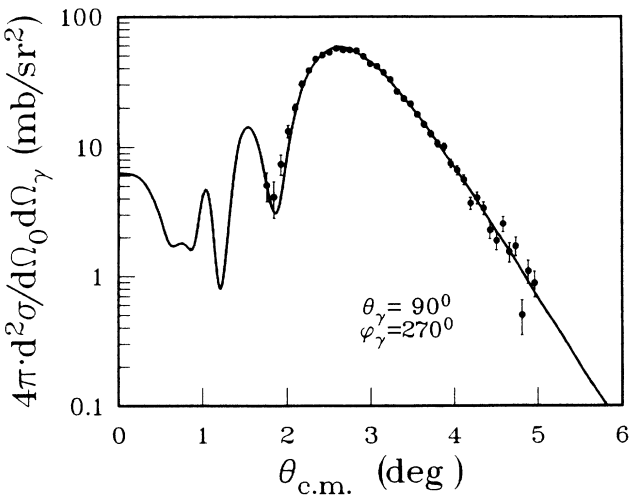


FIG. 7. Angular correlation for the $^{208}$Pb($^{17}$O,$^{17}$O′$\gamma_0$) reaction at 84 MeV/nucleon, for fixed $\gamma$ angle $\theta_\gamma=90°$, $\phi_\gamma=270°$. The points are experimental. The curve is predicted for Coulomb excitation and $E1$ decay of the IVGQR as described in the text.

function of excitation energy using an $E1$ strength distribution taken from photonuclear data[11] and integrated over energy from 9 to 18 MeV to correspond with our data. The distribution of excitation cross section is given by

$$\frac{d\sigma}{d\Omega\, dE}=\left[\frac{d\sigma}{d\Omega}\right]_E b_{E1}(E)\ , \tag{2}$$

where $(d\sigma/d\Omega)_E$ is the DWBA cross section evaluated at excitation energy $E$ for unit $E1$ excitation strength $[B(E1)\uparrow=1\ e^2\text{fm}^2]$, and $b_{E1}(E)=dB(E1)\uparrow/dE$ is the distribution of $E1$ reduced matrix element per unit energy, which can be related to the photonuclear cross section $\sigma_{\text{PN}}(E)$ by

$$b_{E1}(E)=\frac{9\hbar c}{16\pi^3}\frac{\sigma_{\text{PN}}(E)}{E}\ e^2\text{fm}^2/\text{MeV}\ . \tag{3}$$

Since the $E1$ strength is fixed by the photonuclear data,[11] only one free parameter, the branching ratio $R_{\gamma_0}$, remains. It was determined from the fit to the data to be $0.019\pm0.002$.

The absolute yield of ground-state photons can be calculated from the properties of the IVGDR by applying the ideas of the multistep theory of nuclear reactions.[12] This calculation has been described in more detail elsewhere.[13,4] The collective 1p-1h giant dipole state is considered as a doorway state that is strongly excited in the inelastic scattering process. Typically, the giant resonances exist in a region of relatively high density of states into which the doorway strength is mixed or damped. The total width of the resonance is expressed as $\Gamma=\Gamma^{\downarrow}+\Gamma^{\uparrow}+\Gamma_{\gamma_0}$, where $\Gamma^{\uparrow}$ is a width associated with direct decay of the doorway state to excited states (for convenience we separate $\Gamma_{\gamma_0}$, the ground-state photon decay width, explicitly from $\Gamma^{\uparrow}$), and $\Gamma^{\downarrow}$ is a width that describes the damping of the resonance into more complex states.

The giant resonance doorway state damps into the more complex 2p-2h, 3p-3h, etc., states, eventually reaching the fully damped compound state. We consider a single doorway state at energy $E_{\text{GR}}$ with total strength $S_{\text{GR}}$. Following Ref. 13, the cross section for emission of ground-state photons following inelastic scattering can be expressed as

$$\sigma_{x,x'\gamma_0}(E)=\sigma_{x,x'}(E)\left[\sum_{i=1}^{r}\frac{\Gamma_{\gamma_0,i}}{\Gamma_i}\left[\prod_{j=1}^{i-1}\frac{\Gamma_j^{\downarrow}}{\Gamma_j}\right]\right]\ , \tag{4}$$

where $\sigma_{x,x'}(E)$ is the distribution of excitation cross section obtained from a DWBA calculation and the sum in large square brackets runs over the hierarchy of levels of complexity from the doorway stage ($i=1$) to the compound ($r$th) stage. The quantity $\Gamma_i^{\downarrow}$ represents the damping width of the $i$th stage, while $\Gamma_i$ is the total width. The product in large parentheses is a depletion factor that accounts for removal of reactants in stages preceding the $i$th stage. An abbreviated notation has been used in which variables such as the scattering angle of the ejectile ($x'$) and the photon emission angles are suppressed. The $\sigma(E)$ on either side of the equal sign may be considered to represent the multiple differential cross sections in these variables with all the dependence of $\sigma_{x,x'\gamma_0}(E)$ on the various angles contained in $\sigma_{x,x'}(E)$. Application of this general expression requires a great deal of knowledge concerning the various widths associated with each stage. For simplicity we use a two-stage approximation, considering only the GR doorway and the compound states,

$$\sigma_{x,x'\gamma_0}(E)=\sigma_{x,x'}(E)\left[\frac{\Gamma_{\gamma_0}}{\Gamma}+\left[\frac{\Gamma^{\downarrow}}{\Gamma}\right]B_{\text{CN}}(E)\right]\ , \tag{5}$$

where the index 1 for the doorway state has been dropped. $\Gamma$ is identified with the experimental width of the resonance, and $B_{\text{CN}}(E)$ is the compound-nucleus branching ratio. The quantity in large parenthesis preserves unitarity by ensuring that only those systems that survive the damping process ($\Gamma^{\uparrow}$ is the damping width) are included in the compound term. $\Gamma_{\gamma_0}$ is calculated by treating the GR state as a single sharp state at energy $E_{\text{GR}}$. For the IVGDR,

$$\Gamma_{\gamma_0}=\frac{16\pi}{9(\hbar c)^3}E_{\text{GR}}^2 g_I S_{\text{GR}}\ , \tag{6}$$

where

$$g_I=(2I_0+1)/(2I_R+1)\ ,$$

$I_0$ and $I_R$ are the spins of the ground state and the resonance, respectively, and $S_{\text{GR}}$ is the GR strength. For a state exhausting 100% of the classical $E1$ (EWSR),

$$S_{\text{GR}}=14.8\frac{NZ}{A}\ e^2\text{fm}^2/\text{MeV}\ . \tag{7}$$

Experimentally, $S_{\text{GR}}$ can be obtained by integrating the photonuclear cross section [or the derived $b_{E_1}(E)$ from Eq. (2)] over energy:

$$S_{\text{GR}}=\int_{E_1}^{E_2}Eb_{E1}(E)dE\ . \tag{8}$$

The integral in Eq. (8) runs, in principle, over all energies. In practice a finite range must be chosen: We use $E_1$, $E_2=7.5$, 25 MeV, reflecting the range over which $\sigma_{\text{PN}}(E)$ is reliably known.[11] Theoretical and experimental results[14–16] for $^{208}$Pb indicate that $\Gamma^{\uparrow}\gtrsim0.9\Gamma$, so we set the factor $\Gamma^{\downarrow}/\Gamma$ to unity without introducing an uncertainty of more than 10% in the compound contribution. The compound branching ratio can be calculated from mean $\gamma_0$ and total widths obtained from Hauser-Feshbach calculations. It is necessary to include a correction for effects because of the distribution of partial widths that have been discussed extensively in the literature.[17–19] This correction appears as a factor $C$, multiplying the ratio of mean widths:

$$B_{\text{CN}}=C\frac{\langle\Gamma_{\gamma_0,\text{CN}}\rangle}{\langle\Gamma_{\text{CN}}\rangle}\ . \tag{9}$$

The mean $\gamma_0$ widths are given according to statistical theory by

$$\langle \Gamma_{\gamma_0,\mathrm{CN}} \rangle = \frac{\frac{16\pi}{9(\hbar c)^3} g_I b_{E1}(E) E^3}{\rho_I(E)} , \quad (10)$$

where the strength that was assigned to the doorway state before is now distributed in energy over many compound states, and $\rho_I(E)$ is the density of the compound states of the appropriate spin and parity at excitation energy $E$. For the present purposes, contributions to $\langle \Gamma_{\mathrm{CN}} \rangle$, the total compound width, other than $\gamma_0$ and neutron emission are ignored. The mean neutron widths are calculated with the standard Hauser-Feshbach expression using known experimental levels up to ~5 MeV and an empirical level density function[20] for higher energies, and optical-model transmission coefficients.[21] The energy dependent correction factor $C$ in Eq. (9) takes into account width fluctuation and correlation effects as discussed by Moldauer,[17] Lynn,[18] and Axel *et al.*[19] The factor $C$ would be one if all partial widths were constant in a given energy interval (no fluctuation from level to level) or if the fluctuations between the $\gamma_0$ partial widths and the partial widths that dominate $\Gamma_{\mathrm{CN}}$ were completely correlated. It has been shown (see, for example, Ref. 17) that if the form of the distribution of partial widths is specified, $C$ can be obtained directly from quantities that are provided by conventional statistical model calculations, namely the ratio of average widths $\langle \Gamma_{\gamma_0} \rangle / \langle \Gamma \rangle$ and the number of open channels that contribute to $\langle \Gamma \rangle$. We calculate $C$ under the assumption that both the $\gamma_0$ partial widths and the neutron partial widths that dominate $\Gamma^{\mathrm{CN}}$ are distributed according to Porter-Thomas distributions. All other information required comes from a standard statistical-model calculation.

The solid line in Fig. 8 compares the results of applying the aforementioned formalism to the measured ground-state photon decay of the IVGDR. The distribution of excitation cross section in energy and angle was calculated as discussed earlier Eq. (2) in the DWBA using the code PTOLEMY,[22] considering only Coulomb excitation. These calculations were carried out at 1 MeV intervals, then interpolated in energy and integrated over the $^{17}$O scattering angle range appropriate to the data. The excitation strength distribution was taken directly from the experimental photonuclear cross section.[11] There are no free parameters (since we set $\Gamma^{\downarrow}/\Gamma = 1$). The experimental ($^{17}$O,$^{17}$O$'\gamma_0$) spectrum (points with error bars) is the same as in Fig. 5. The dashed line gives the separate contribution of the first term (primary doorway) in Eq. (5), while the dotted line gives the contribution of the second (compound) term. The agreement between the data and the calculation is excellent. It should be noted that the data above ~14 MeV are well described by the first term in Eq. (5), which implies a ground-state photon branching ratio independent of excitation energy. The energy-averaged total photon branch, integrated over the energy interval 9.5–25 MeV gives $R_{\gamma_0} = 0.017$, in remarkable agreement with the value of $0.019 \pm 0.002$ deduced from the fit of the angular correlation in Fig. 7.

The calculation ignored all contributions other than the IVGDR to ground-state photon production in the 9–25 MeV region. Application of the formalism to other resonances clearly demonstrates that this is a very good assumption: Ground-state decay of the ISGQR makes about a 1% contribution over the energy interval considered. Higher multipoles contribute at the 1 in $10^3$ level or less.

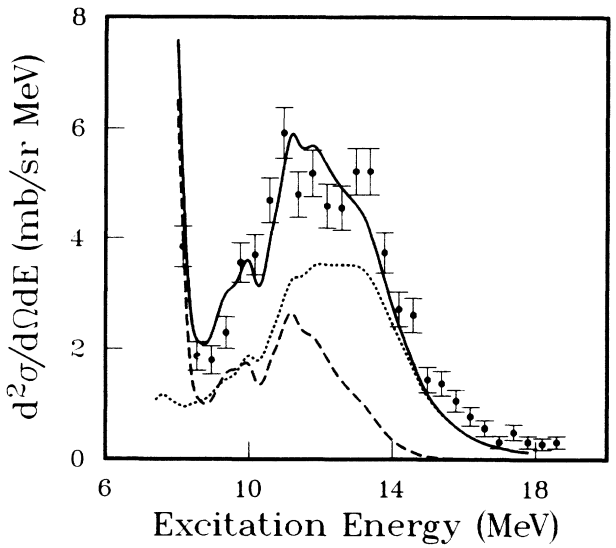


FIG. 8. The ground-state gamma coincidence yield for 84 MeV/nucleon $^{17}$O scattering on $^{208}$Pb, compared with calculations. The solid curve is the full result of calculations using Eq. (2), while the dotted curve gives the separate contribution of the first (direct) term of Eq. (2) and the dashed line gives the contribution of the second (compound) term in Eq. (2).

### B. Analysis of the giant resonance region of the inelastic spectra

Since the measured ground-state photon spectra of the IVGDR can be quantitatively understood by the calculations described in Sec. III A, we have used these results to analyze also the inelastic singles spectra. In Fig. 9 we show the decomposition of the 3.00° singles spectrum as an example of the procedure we have followed. The continuum underlying the giant resonances was subtracted from the inelastic spectrum at each angle of measurement. The shape for the continuum was taken to be a third-order polynomial above an excitation energy of 12 MeV; for lower energies the polynomial was matched to a Gaussian peak centered at 12 MeV with an energy dependent amplitude that tended toward zero at the neutron separation energy. A similar phenomenological shape for the continuum was used in analyses of inelastic hadron scattering.[23] The polynomial was fitted to the data at $E_x \geq 30$ MeV. Figure 9(a) shows the full singles spectrum with a solid line representing the assumed underlying continuum. The histogram in Fig. 9(b) shows the same spectrum as in Fig. 9(a) after the subtraction of the continuum. The double differential cross section, $d^2\sigma/d\Omega\, dE$, for Coulomb excitation of the IVGDR was calculated as a function of $^{17}$O scattering angle and excitation energy as discussed in Sec. III A [see Eq. (2)]. The distribution of IVGDR cross section in excitation energy

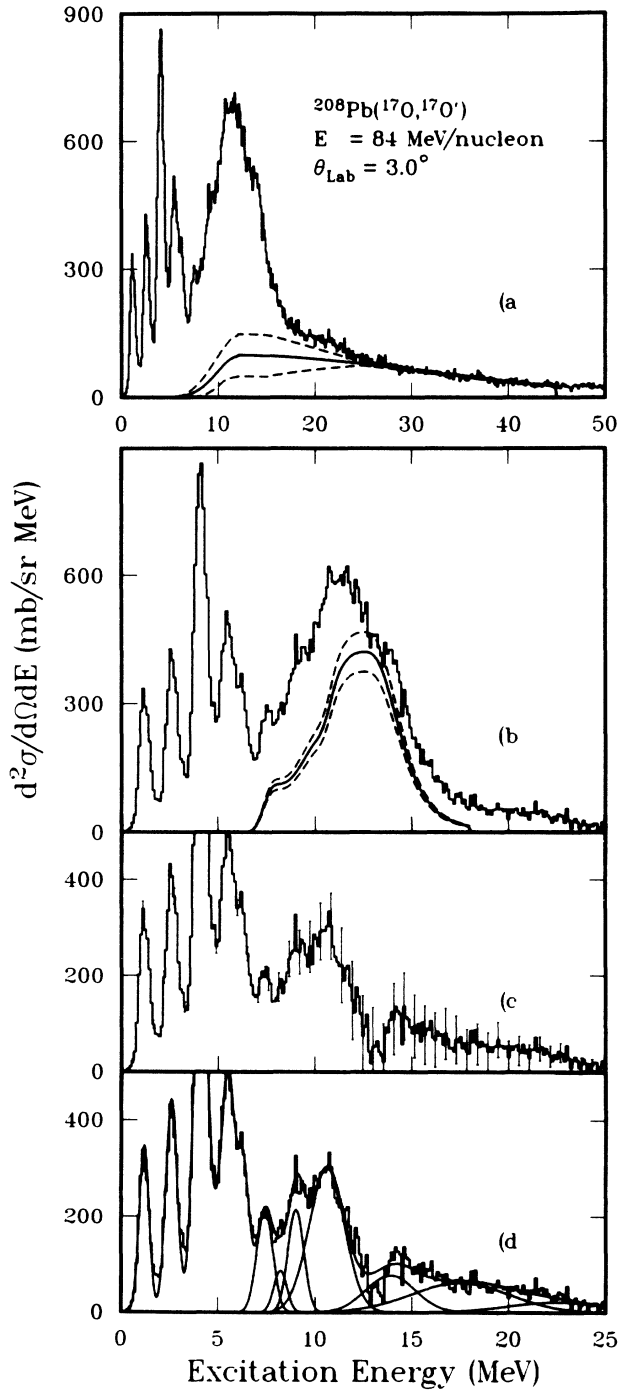


FIG. 9. Decomposition of singles spectrum at $\theta = 3.00°$ from the $^{208}$Pb($^{17}$O,$^{17}$O') reaction at 84 MeV/nucleon. (a) Full singles spectrum (histogram) with solid line showing assumed shape and magnitude of the underlying continuum. The dashed curves are discussed in the text. (b) Histogram showing the same spectrum as after subtraction of assumed continuum, with solid curve giving the calculated shape of the IVGDR. The dashed curves are discussed in the text. (c) Spectrum from (b) following subtraction of IVGDR; error bars are shown indicating the combined uncertainty as discussed in the text on representative points. (d) Spectrum from (c) fitted with peaks as discussed in the text and shown in Table I.

depends quite sensitively on the scattering angle. For each experimental scattering angle, the calculated double differential cross section was integrated over the solid angle corresponding to that defined by the cuts used to construct the experimental spectra. Calculated shapes for the IVGDR for scattering angles of $\theta_{c.m.} = 2°$ (dash) and 3° (dot) are shown along with the photonuclear strength function (solid curve) in Fig. 10. The curves in Fig. 10 are normalized to unit area over the 7–25 MeV interval so they will fit on the same plot. The integrated cross sections for the 2° and 3° spectra are 425 and 2245 mb/sr, respectively. The photonuclear curve exhausts 117% of the isovector, $L=1$, EWSR. The IVGDR shape appropriate to the data in Fig. 9 is shown as the solid curve in Fig. 9(b).

Figure 9(c) shows the spectrum of Fig. 9(b) after subtraction of the IVGDR peak. The difference spectrum clearly shows the presence of two broad excitations, one near 10 MeV and the other near 14 MeV, the energies of the ISGQR and ISGMR, respectively. The structure near 10 MeV shows at least two components, one at 10.6 MeV and another at ~9 MeV. Inelastic proton scattering with good energy resolution has shown[7] that the 10.6-MeV peak is 2 MeV wide and exhausts ~70% of the isoscalar, $L=2$, EWSR. In addition, the $(p,p')$ work finds narrow quadrupole states located at 7.36, 7.84, 8.86, and 9.34 MeV, each having a width of ~400 keV and depleting a total of 20–25 % of the EWSR. The only other peaks reported in Ref. 7 in the 7.5–11-MeV range were at excitation energies of 8.1 and 8.3 MeV and were identified as $L=3$ and $L=4$, respectively, each exhausting a few percent of the relevant EWSR. The ISGMR is represented by a peak at 13.9 MeV with a 2.9-MeV width. Figure 9(c) also shows peaks corresponding to excitation of well-known states at 2.613 MeV ($3^-$) and

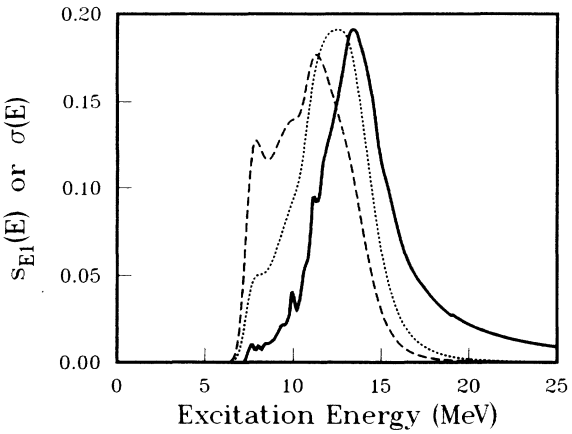


FIG. 10. Isovector giant dipole resonance shapes versus scattering angle. The solid curve is the giant dipole resonance strength function from photonuclear reactions (Ref. 11). The dashed and dotted curves are, respectively, the 2° and 3° distributions of excitation cross section for the IVGDR resulting from Coulomb excitation in the $^{208}$Pb($^{17}$O,$^{17}$O') reaction at 84 MeV/nucleon. For display purposes, these curves are normalized to have unit energy integrals.

4.085 MeV ($2^+$). Figure 9(d) shows the spectrum from Fig. 9(c) fitted with all the peaks just mentioned for the region above 2 MeV of excitation energy. In the fitting process we have used the peak locations and widths from the high resolution $(p,p')$ measurements; only the area of the peaks was allowed to vary. The pairs of states at 7.4+7.8 MeV and 8.9+9.3 MeV were treated as single peaks at ~7.5 and ~9.1 MeV because of the 800-keV energy resolution in the present experiment. The fit was improved by including a peak at 8.2 MeV corresponding to the 8.1+8.4 MeV states of Ref. 7. However, the fit results for the cross sections of the nearby $L=2$ states was independent, within fitting uncertainties, of whether this peak was included. As is evident from Fig. 9(d) this procedure provides an excellent fit to the spectrum. Table I lists the energies, widths, and deduced strengths of the peaks between 7 and 16 MeV used in the fitting procedure. The differential cross sections for elastic scattering and inelastic excitation of the 2.61- and 4.085-MeV states have been discussed in Ref. 6. To account for the cross section above the ISGMR, peaks at 17.0 and 23.0 MeV were also included; resonances in $^{208}$Pb near these excitation energies have been reported in the literature.[1,5]

Differential cross sections for the peaks located at ~7.5 (7.33+7.84), ~9.1 (8.86+9.34), 10.6, and 13.9 MeV are shown by the points in Fig. 11. The solid curves are the results of distorted-wave calculations using the code PTOLEMY[22] utilizing the $L$ transfers determined in inelastic light-ion scattering.[7] Optical-model parameters were obtained from a fit to our elastic scattering data as discussed in Ref. 6. The angular distribution for the 7.3+7.8-MeV peak should contain some $L=1$ contribution from Coulomb excitation of the known[24] $1^-$ states in this energy region. However, inclusion of $L=1$ strength[24] of $B(E1)\uparrow=0.002\ e^2b$ makes no improvement to the pure $L=2$ calculation shown on Fig. 11.

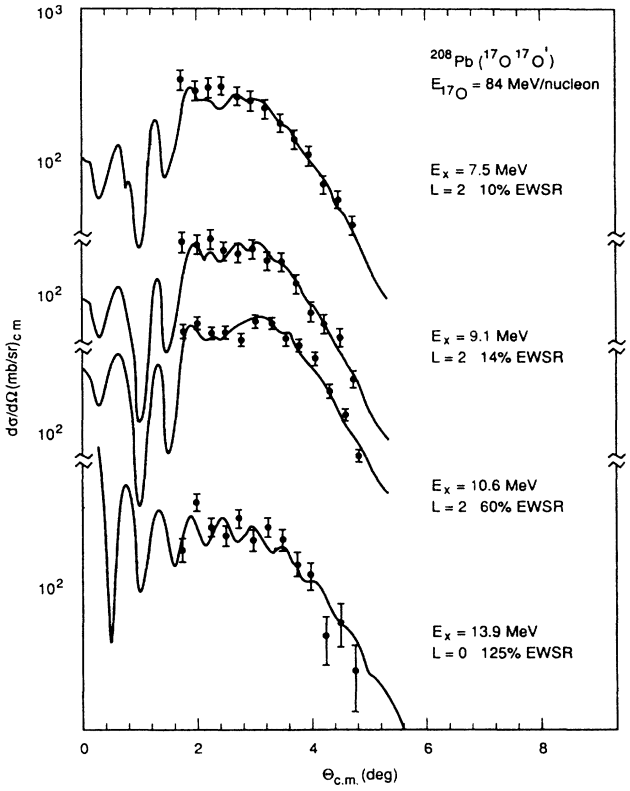


FIG. 11. Measured and DWBA calculated differential cross sections for states in the excitation energy range of ~7–14 MeV excited in the $^{208}$Pb($^{17}$O,$^{17}$O') reaction for 84-MeV/nucleon $^{17}$O ions.

A precise assessment of the uncertainties on the cross sections deduced from this analysis is difficult, but since a quantitative estimate is essential to establish the significance of the analysis carried out in the next section, an effort has been made to establish a conservative limit on these uncertainties. Besides the usual counting statistics, there are four principal sources of uncertainty in the analysis: (1) the overall normalization, (2) the IVGDR contribution, (3) the continuum subtraction, and (4) peak fitting uncertainties. An overall normalization uncertainty of ±10% results from lack of precise knowledge of basic characteristics of the experimental setup (target thickness, beam current integration, solid angle, etc.). The IVGDR is included in the analysis as an absolute cross section based on photonuclear data. We have demonstrated with the gamma-decay coincidence data that the excitation of the IVGDR is quantitatively understood in terms of the photonuclear data used as input to a DWBA calculation, considering only the Coulomb excitation process. The uncertainty in the IVGDR contribution is thus a combination of the ±5% uncertainty in the photonuclear data itself,[11] the ±10% uncertainty in our absolute cross section scale and the uncertainty associated with the Coulomb excitation calculation, which is negligible compared to the other effects. The overall uncertainty range of the IVGDR contribution is indicated by the two dashed curves on Fig. 9(b) that lie on either side of the heavy solid curve (the best estimate). The shape and magnitude of the continuum, shown as a solid curve in Fig. 9(a), is not well constrained by theoretical considerations, and is hence to some extent arbitrary. A conservative estimate of the range of uncertainty in this background curve is shown by dashed curves on Fig. 9(a), and ranges from 100% at threshold to ~50% at the peak of the 10.6-MeV GQR. This empirical background problem is shared with all other experiments involving hadronic excitation of giant resonances. An important

TABLE I. Properties of analyzed continuum states. FWHM denotes full width at half maximum.

| $E_x$ (MeV) | FWHM (MeV) | $L$ | Percent of EWSR This work | Ref. 7 |
|---|---|---|---|---|
| 7.36 | 0.8 | 2 | 10±2 | 6.5±1.0 |
| 7.84 | | | | 4.2±0.6 |
| 8.86 | 0.8 | 2 | 14±3 | 7±1 |
| 9.34 | | | | 5±0.8 |
| 10.6 | 2.0 | 2 | 60±9(6) | 70±14 |
| 13.9 | 2.9 | 0 | 125±44(25) | 100 |

feature of the present data is the small size of the continuum relative to the resonance peaks. Over the region occupied by the GQR (9–12 MeV), the average background is 65 mb/MeV, compared to a peak GQR yield of 300 mb/MeV at 10.6 MeV.

The error bars shown on Fig. 9(c) indicate the uncertainties on individual data points resulting from the combination of counting statistics of the continuum subtraction and IVGDR effects discussed earlier. Since these combined uncertainties vary considerably across peaks fitted in the analysis, these uncertainties were used in the fitting procedure. The cross section uncertainties which result from these fits are shown on Fig. 11.

This procedure underestimates the overall uncertainty in the deduced cross sections, since the uncertainties in the continuum and IVGDR cross sections cannot be considered random quantities that fluctuate from data point to data point, but as systematic effects that affect a range of nearby data points in a correlated way. The size of this effect was estimated by redoing the analysis with the extreme range of values for these quantities shown in Fig. 9(a) and (b). Of the peaks of particular interest here, only the uncertainties for those at 10.6 and 13.9 MeV were significantly affected by this procedure. The resulting uncertainty on the 10.6-MeV cross section ranged from 10% to 18% for the various angles considered. For the 13.9-MeV ISGMR, uncertainties on points inside of 3.5° are increased substantially from those shown on Fig. 11 to about 35%.

Table I shows the values for the EWSR depletion from the present work along with those from the $(p,p')$ high-resolution measurements.[7] Two estimates for the uncertainty on the 10.6-MeV GQR and 13.9-MeV ISGMR are shown. The values in parenthesis neglect the effect of estimated uncertainty in the continuum, while the other values include the combination of all effects discussed in the preceding paragraph. It is clear that the two experiments are in excellent agreement.

The only resonance reported in the $(p,p')$ work but not observed here is a hexadecapole resonance (ISGHR) located at 12.0 MeV with $\Gamma=2.4$ MeV, which exhausts $\sim 10\%$ of the EWSR. Excitation of such a resonance in the present work would produce a cross section of $\sim 70$ mb/sr near the maximum of the angular distribution. A peak of this shape and magnitude would be largely masked by the ISGQR and ISGMR, but there were indications of some excess cross section near 12 MeV at a few angles, so that we cannot say that our data contradict Ref. 7. For example, if such a peak at 12 MeV is included in the fit to the 3° data shown in Fig. 9, the corresponding best fit cross section is 3 mb/sr, with an uncertainty of $\pm 80$ mb/sr. Inclusion of this $L=4$ excitation with a fixed cross section corresponding to 10% of the EWSR would reduce the ESWR strength for the 10.6-MeV $L=2$ state by less than 5% from that shown in Table I, and would reduce the $L=0$ strength at 13.9 MeV deduced from our data by 13%.

### C. The isospin character of the 10.6-MeV GQR

In analysis of hadron scattering experiments on giant resonances (including that in the previous section), one usually assumes a fixed relationship between the strength of the electromagnetic and hadronic excitations, which amounts to an assumption about the isospin character of the state being excited. Recent $\pi^+$ and $\pi^-$ scattering data[25] on the 10.6-MeV GQR in $^{208}$Pb have suggested that the usual assumption that the state is purely isoscalar is in error; rather those results suggest that the 10.6-MeV GQR is predominantly a neutron excitation and consequently of mixed isospin character. In general, determination of the relative proton and neutron contributions to an excitation has been based on comparison of two measurements using scattering of probes with different isospin sensitivity (e.g., $\pi^+$ and $\pi^-$ or $p$ and $n$). Alternatively, electromagnetic excitation $(e,e')$ can be compared with excitation by a nuclear probe, e.g., $(\alpha,\alpha')$. On the other hand, it has been pointed out several times in the literature that Coulomb-nuclear interference effects in hadron scattering can be used to determine relative proton and neutron contributions from a single measurement.[26–29] Our data on the 10.6-MeV GQR are particularly favorable for such an analysis because of the strong contribution of Coulomb excitation at 84 MeV/nucleon. In this section we will outline the formalism used in extracting this information from our data.

It is convenient to express the isospin character of a collective nuclear excitation in terms of the ratio of neutron to proton matrix elements $M_n/M_p$, where

$$M_i = \int g_L^i(r) r^{L+2} dr \tag{11}$$

and $i$ takes on the values $n$ (neutron) and $p$ (proton). The $g_L^i(r)$ is the neutron or proton transition density.[29] $M_p$ is related to the conventional electromagnetic reduced transition probability, $B(EL)\uparrow$, by

$$B(EL)\uparrow = |M_p|^2 e^2 . \tag{12}$$

Satchler[30] has defined a mass reduced transition probability, $B(L)\uparrow$ that we can also relate to the $M_i$;

$$B(L)\uparrow = |M_n + M_p|^2 . \tag{13}$$

If the quantities $B(L)\uparrow$ and $B(EL)\uparrow$ can be extracted from the experiment then

$$|M_n/M_p| = \left[ \frac{B(L)\uparrow}{B(EL)\uparrow/e^2} \right]^{1/2} - 1 . \tag{14}$$

For the simplest collective mass oscillation, which one would expect to apply to a giant resonance state exhausting a large fraction of the EWSR, one expects $M_n/M_p \sim N/Z$ (1.54 for $^{208}$Pb). The pion scattering results[25] give $|M_n/M_p| \sim 3.8$.

We have analyzed our data using the deformed potential model[2,29,30] with the DWBA code PTOLEMY.[22] The transition potential $G_L$ for excitation of a collective state of angular momentum $L \geq 2$ is given by the sum of a nuclear and Coulomb part[2,30]

$$G_L(r) = G_L^N(r) + G_L^C(r) ,$$

where

$$G_L^N(r)=\delta_L \frac{dU(r)}{dr} ,$$
$$G_L^C(r)=\pm[B(EL)\uparrow]^{1/2}V_C(r) , \quad (15)$$

and

$$V_C(r)=\frac{4\pi Z'e^2}{2l+1}\times\begin{cases}1/r^{l+1}, & r\geq R_C\\ \dfrac{r^l}{R_C^{2l+1}}, & r<R_C\end{cases} .$$

$U(r)$ is the optical potential determined from fitting the elastic scattering, $Z'$ is the atomic number of the projectile, $R_C$ is a charge radius parameter that plays no role here since contributions from $r<R_C$ are negligible, and $\delta_L$ is the hadronic deformation length, which measures the strength of the hadronic excitation.[30] The sign of the Coulomb term is positive if the transition is predominantly isoscalar ($M_n/M_p>0$) and negative otherwise.

The Coulomb part of the transition potential [Eq. (15)] is expressed explicitly in terms of $B(EL)\uparrow$. The problem that remains is to relate $\delta_L$ to $B(L)\uparrow$. This is not straightforward, particularly for a potential model analysis such as that carried out here, since we have no well defined way to relate the collective model transition potentials to the transition densities that appear in Eq. (11). We make the association by assuming, following the discussion given by Satchler,[30] that the deformation length, $\delta_L$, in Eq. (15) is related to the deformation and radius of the nuclear density distribution by

$$\delta_L=\beta_L R .$$

The expression for $B(L)\uparrow$ appropriate to the form of the transition density potential of Eq. (15) is then[30]

$$B(L)\uparrow=\delta_L^2\left[\frac{A(L+2)}{4\pi}\langle r^{L-1}\rangle\right]^2 , \quad (16)$$

where $\langle r^K\rangle$ is the $K$th radial moment of the nuclear density distribution $\rho(r)$:

$$\langle r^K\rangle=\int\rho(r)r^{K+2}dr\Big/\int r^2\rho(r)dr ; \quad (17)$$

for a density distribution given by a Fermi function of half-density radius $C$ and diffuseness parameter $a$,

$$\langle r^K\rangle\approx\frac{3}{K+3}\left[C+\frac{\pi^2(K+5)a^2}{6C}\right]^K . \quad (18)$$

The isoscalar EWSR limit for $\delta_L$ for an excitation with $L\geq 2$ at excitation energy $E$ in a nucleus with a uniform density distribution and mass number $A$ is[2,30]

$$\delta_L^2=\frac{2\hbar L(2L+1)}{3AmE} , \quad (19)$$

where $m$ is the nucleon mass.

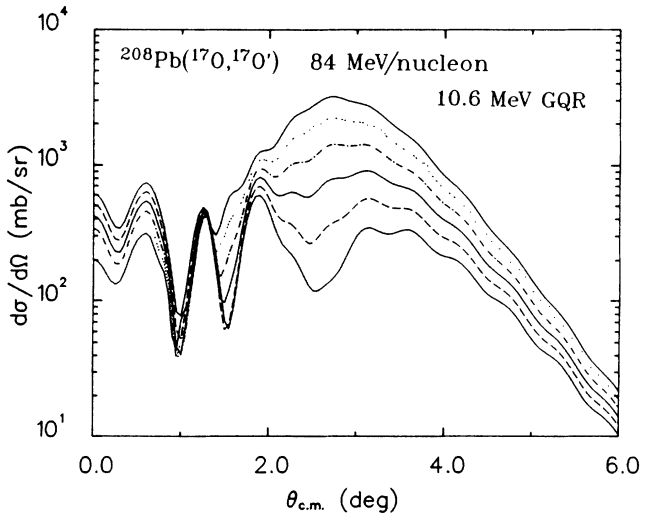


FIG. 12. Calculated angular distributions for the reaction $^{208}$Pb($^{17}$O,$^{17}$O′) at 84 MeV/nucleon illustrating the sensitivity to the ratio $M_n/M_p$. The cross sections increase monotonically with decreasing $M_n/M_p$ for angles greater than $\sim 2°$. The curves are for values of $|M_n/M_p|$ of 4.3, 2.5, 1.7, 1.1, 0.8, and 0.5 (in order of increasing cross sections). The hadronic sum rule strength, proportional to $|M_n+M_p|^2$, is the same (100% of EWSR) for all curves.

The experimental data for the 10.6-MeV angular distribution was fit to the two parameters $B(L)$ (i.e., $\delta_L$) and $M_n/M_p$ simultaneously. In practice, calculations were done for $B(L)$ fixed at the value determined by the EWSR for a range of values of $M_n/M_p$ from $\sim 0.5$ to $\sim 4$, utilizing the relation between $B(L)\uparrow$ and $B(EL)\uparrow$ given by Eq. (14) to construct the transition potential. The resulting angular distributions were then each fitted to the experimental data by adjusting an overall normalization factor, making use of the fact that in the DWBA $d\sigma/d\Omega\propto|G_L(r)|^2$. The sensitivity of the data to the $M_n/M_p$ ratio is illustrated in Fig. 12, which shows the calculated differential cross sections for constant $\delta_L$ and

TABLE II. Coulomb nuclear interference analysis of the 10.6-MeV GQR.

| | $\lvert M_n/M_p\rvert$ | $B(E2)\uparrow$ | $B(N2)\uparrow$ | $f$ (EWSR) (%) |
|---|---|---|---|---|
| This work (10.6 only) | 1.7±0.4 | 3980±440 | 10 800±3560 | 61±15 |
| This work (10.6+9.3+8.9) | | 5120±840 | 13 500±4503 | 74±17 |
| $\pi,\pi'$ (Ref. 24) | 3.8 | 1010±600 | 14 500±3600 | 48±7 |
| $(e,e'n)$ (Ref. 31) | | 5400±1350 | | 67±17 |

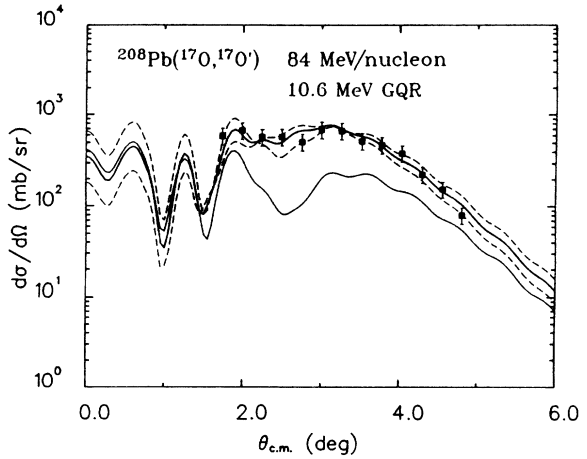


FIG. 13. Comparison of the differential cross sections from the present measurement for excitation of the 10.6-MeV GQR (points) with the best-fit calculated angular distribution. The dashed curves show the calculated angular distribution using $M_n/M_p$ values that differ by one standard deviation from the best-fit value. Also shown (lower full curve) is the angular distribution calculated using the $M_n/M_p$ values from the inelastic pion scattering data of Ref. 25. The uncertainties shown on the data points reflect the effects of continuum subtraction and the IVGDR, as well as peak fitting uncertainties, as discussed in the text.

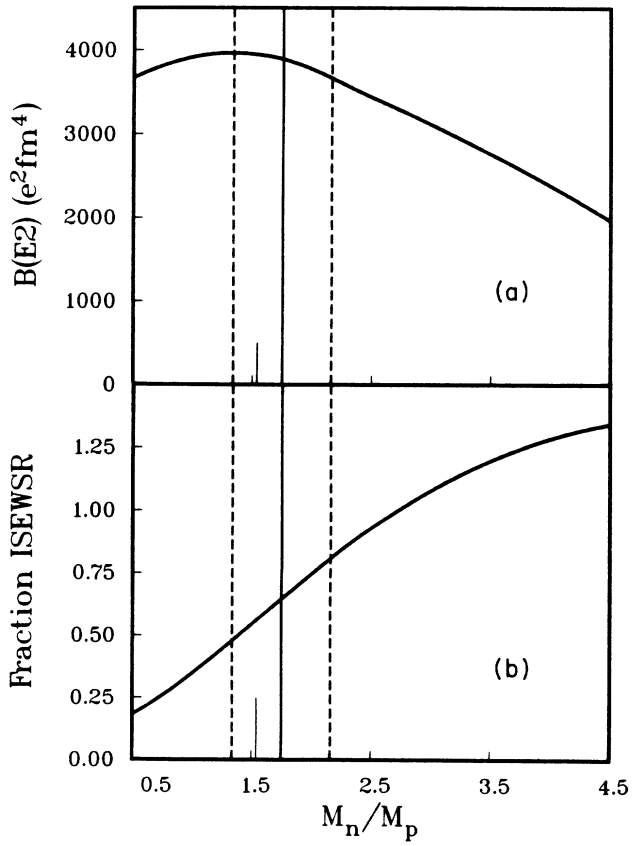


FIG. 14. Variation of (a) $B(E2\uparrow)$ and (b) $\delta_2/\delta_2$(EWSR) for excitation of the 10.6-MeV GQR state as a function of $M_n/M_p$ for local best-fit calculations matching the data from the present experiment. The vertical line shows the overall best fit and the dashed lines mark the one-standard-deviation limits.

representative $M_n/M_p$ values. Best-fit values of $B(EL)\uparrow$ and $M_n/M_p$ are shown in Table II along with the quantity $B(NL)\uparrow$, which is a reduced neutron transition probability defined analogously to $B(L)\uparrow$ and $B(EL)\uparrow$. The column labeled $f$ (EWSR) gives the ratio of the best fit $\delta_L$ to the value calculated from Eq. (19). The corresponding best-fit curve is shown in Fig. 13 along with the curve obtained using the $M_n/M_p$ result of the pion scattering experiment.[25] The dashed curves show the calculated angular distribution using $M_n/M_p$ values that differ by one standard deviation from the best-fit value. The solid lower curve is calculated using the $M_n/M_p$ ratio from Ref. 25. Figure 14 shows the variation of the local best-fit values of $B(E2)\uparrow$ and $\delta_2/\delta_2$(EWSR) as a function of $M_n/M_p$ as determined in the fits. The heavy vertical line marks the best-fit value for $M_n/M_p$ (1.7) and the light vertical lines mark the one standard deviation range ($\pm 0.4$) in $M_n/M_p$. This illustrates that our measurement determines $B(E2)\uparrow$ for the 10.6-MeV GQR almost independent of $M_n/M_p$, because of the large role played by Coulomb excitation at this bombarding energy. The value of $M_n/M_p$ determined here is less than half of that reported in Ref. 25 and our value of $B(E2)\uparrow$ for the 10.6-MeV GQR of $3980\pm440$ $e^2/\text{fm}^4$ is almost 4 times larger than the value reported in Ref. 25. This does not include the additional $E2$ strength that we find at $\sim 8.9$ and $\sim 9.3$ MeV, and that is presumably included in the 10.6-MeV peak in the analysis in Ref. 25. Also included in Table II is an estimate of the total $L=2$ strength in the GQR region, made by including the 8.8- and 9.3-MeV $2^+$ states (Sec. III B) with the 10.6-MeV state. Since an explicit analysis in terms of $M_n/M_p$ was not carried out for the 8.8+9.3-MeV peak, we have assumed $M_n/M_p = 1.54\pm0.40$ ($N/Z\pm25\%$) for this component.

From our results shown in Fig. 13 we deduce $M_n/M_p = 1.7\pm0.4$, while $N/Z = 1.54$. We conclude that the GQR state at 10.6 MeV in $^{208}$Pb has a character consistent with that expected of an in-phase oscillation of neutrons and protons—i.e., a collective isoscalar vibration. This result is in agreement with inferences from other hadron inelastic scattering experiments[1] and with recent measurements[4] of the photon decay of the GQR.

### D. Comparison with electron scattering

There has been a long standing disagreement between results for the integrated strength of the isoscalar GQR obtained in hadron scattering and electron scattering experiments. This fact was cited in Ref. 25 as support for the large value of $M_n/M_p$ obtained in that work. Recently a coincidence electron scattering experiment[31] $(e,e'n)$ has been reported for the GQR region in $^{208}$Pb. Since we have explicitly determined the electromagnetic strength in our analysis, we can make a direct comparison of the distribution of $B(E2)\uparrow$, as shown in Fig. 15. The data points are from the $(e,e'n)$ data of Ref. 31, while the solid line is the $B(E2)\uparrow$ distribution determined from the analysis of our heavy-ion inelastic scattering data. We include the contribution of the 8.8- and 9.3-MeV $E2$ states for which $B(E2)\uparrow$ was calculated from the analysis of Sec. III B assuming $M_n/M_p = N/Z$.

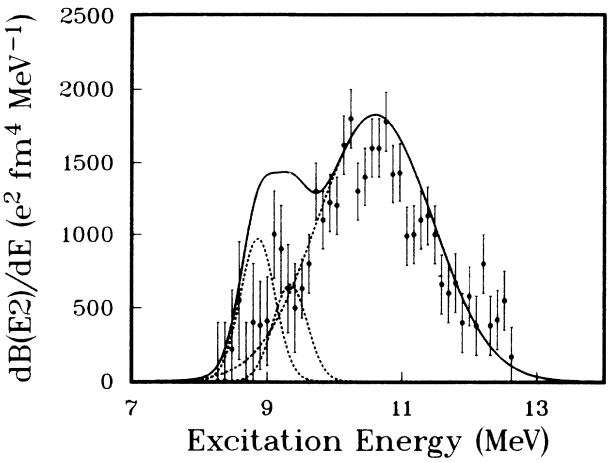


FIG. 15. The distribution of $B(E2)\uparrow$ in the giant resonance region as obtained from the present measurements (solid curve) and the $(e,e'n)$ movements of Ref. 31 (points with error bars). The contributions of the 8.8- and 9.3-MeV states and the 10.6-MeV state are shown separately as dashed curves.

The integrated $B(E2)\uparrow$ strength from our data for the entire GQR region ($\sim$8–13 MeV) shown in Fig. 15 is $5120\pm800\ e^2\text{fm}^4$, in good agreement with the corresponding value ($5400\ e^2\text{fm}^4$) reported from the $(e,e'n)$ measurement of Ref. 31. It is also clear from Fig. 15 that not only is the integrated $B(E2)\uparrow$ consistent for the two data sets but also the distribution of $B(E2)\uparrow$ strength is in excellent agreement over the bulk of the 10.6-MeV GQR.

## IV. CONCLUSIONS

We have presented a detailed analysis of the distribution of ground-state photon decay cross section in both energy and angle, following inelastic excitation of $^{208}$Pb by 84-MeV/nucleon $^{17}$O. Our results show that both the qualitative and quantitative properties of this cross section are predicted in detail using standard methods for the treatment of excitation of the IVGDR considering only Coulomb excitation and the IVGDR strength distribution from photonuclear data. These results fix experimentally the dominant IVGDR peak of the singles spectrum.

Previous analysis of the giant resonance singles spectrum from the present experiment involved a decomposition into six peaks as described in Ref. 6. Although clearly not unique, the decomposition in Ref. 6 is consistent with the best existing light-ion inelastic scattering data. In the present work we have isolated the IVGDR by studying coincidences with photons to the ground state, and have thereby determined the angular and energy distribution of the IVGDR in a way that is completely independent of the contribution of other multipolarities. This *experimental* isolation of the IVGDR allows us to fix the dominant contribution to the resonance peak in the decomposition of the singles spectrum. In this way, we have been able to deduce angular distributions for the ISGQR and ISGMR that are essentially free of uncertainty due to covariance with the IVGDR component. This procedure, coupled with the increased accuracy of continuum removal provided by the extremely large peak to continuum ratio of these data, leads to significantly reduced uncertainties on the differential cross sections for the 10.6-MeV GQR.

The increased accuracy of the angular distribution for the GQR extracted in the present analysis has been used to address two important, long-standing issues concerning the GQR in $^{208}$Pb. First, because the GQR is strongly Coulomb excited as well as nuclear excited we can deduce the ratio of neutron to proton matrix elements ($M_n/M_p$) with a high degree of sensitivity (Fig. 12). We find a value $M_n/M_p = 1.7\pm0.4$, which indicates the 10.6-MeV GQR is an isoscalar state. This result is in sharp contrast to recently published results[25] from $\pi^+$ and $\pi^-$ inelastic scattering. Second, we provide for the first time a quantitative comparison between the $E2$ GR strength distribution from hadronic excitation with that from electron scattering. We find excellent agreement, both qualitatively and quantitatively, between the two measurements.

We believe the results in the present paper clearly demonstrate that heavy-ion scattering near 100 MeV/nucleon can be a powerful and precise tool for investigating isovector strength in the giant resonance region. Because of the extremely large cross sections from Coulomb excitation and the accuracy with which the IVGDR excitation process can be treated, medium energy heavy-ion inelastic scattering provides a way to study details of the IVGDR that is at least competitive to the cleanest present technique, that of tagged photon scattering.

## ACKNOWLEDGMENTS

This research was sponsored by the U.S. Department of Energy, under Contract No. DE-AC05-84OR21400 with Martin Marietta Energy Systems, Inc. We thank the members of the professional and technical staffs of the Grand Accélérateur National d'Ions Lourds (GANIL) facility for their help, hospitality, and efficient delivery of the high quality beams required for our measurements.

*Present address: Foster Radiation Laboratory, McGill University, 3610 University Street, Montreal, Quebec, Canada H3A 2B2.

[1]F. E. Bertrand, Nucl. Phys. **A354**, 129c (1981).
[2]G. R. Satchler, Nucl. Phys. **A472**, 215 (1987).
[3]F. E. Bertrand, J. R. Beene, and D. J. Horen, Nucl. Phys. **A488**, 163c (1988).
[4]J. R. Beene, F. E. Bertrand, M. L. Halbert, R. L. Auble, D. C. Hensley, D. J. Horen, R. L. Robinson, R. O. Sayer, and T. P. Sjoreen, Phys. Rev. C **39**, 1307 (1989).
[5]F. E. Bertrand, R. O. Sayer, R. L. Auble, M. Beckerman, J. L. Blankenship, B. L. Burks, M. A. G. Fernandes, C. W. Glover,

E. E. Gross, D. J. Horen, J. Gomez del Campo, D. Shapira, and H. P. Morsch, Phys. Rev. C **35**, 35 (1987).

[6]J. Barrette, N. Alamanos, F Auger, B. Fernandez, A. Gillibert, D. J. Horen, J. R. Beene, F. E. Bertrand, R. L. Auble, B. L. Burks, J. Gomez del Campo, M. L. Halbert, R. O. Sayer, W. Mittig, Y. Schutz, B. Haas, and J. P. Vivien, Phys. Lett. B **209**, 182 (1988).

[7]F. E. Bertrand, E. E. Gross, D. J. Horen, R. O. Sayer, T. P. Sjoreen, D. K. McDaniels, J. Lisantti, J. R. Tinsley, L. W. Swenson, J. B. McClelland, T. A. Carey, K. Jones, and S. J. Seestrom-Morris, Phys. Rev. C **34**, 34 (1986).

[8]F. A. Beck, in *Instrumentation for Heavy Ion Nuclear Research,* edited by D. Shapira (Harwood Academic, New York, 1985), p. 129.

[9]R. Brun, F. Bruyant, A. C. McPherson, and P. Zanarini, GEANT3 Users Guide, CERN Report No. DD/EE/84-1, 1986 (unpublished).

[10]J. Raynal, Phys. Rev. C **23**, 2571 (1981).

[11]A. Veyssiere, H. Beil, R. Bergere, P. Carlos, and A. Lepretre, Nucl. Phys. **A159**, 561 (1979); see also B. L. Berman and S. C. Fultz, Rev. Mod. Phys. **47**, 713 (1975).

[12]H. Feshbach, A. Kerman, and S. Koonin, Ann. Phys. (N.Y.) **125**, 429 (1980); M. Hussein, and K. McVoy, Phys. Rev. Lett. **43**, 1645 (1979); H. Dras, M. S. Hussein, and S. K. Adhikari, *ibid.* **57**, 1998 (1986).

[13]J. R. Beene, G. F. Bertsch, P. F. Bortignon, and R. A. Broglia, Phys. Rev. Lett. **164B**, 19 (1985).

[14]G. F. Bertsch, P. F. Bortignon, and R. A. Broglia, Rev. Mod. Phys. **55**, 287 (1983).

[15]G. J. Wagner, in *Giant Multipole Resonances,* edited by F. E. Bertrand (Harwood Academics, New York, 1980), pp. 251–274.

[16]L. S. Cardman, Nucl. Phys. **A354**, 173c (1981).

[17]P. A. Moldauer, Phys. Rev. C **11**, 426 (1975).

[18]J. E. Lynn, *Theory of Neutron Resonance Cross Sections* (Oxford University, Oxford, 1968).

[19]P. Axel, K. K. Min, and D. C. Sutton, Phys. Rev. C **2**, 689 (1970).

[20]A. Gilbert and A. G. W. Cameron, Can. J. Phys. **43**, 1446 (1965).

[21]J. Rapaport, J. Kulkarni, and R. W. Finlay, Nucl. Phys. **A330**, 15 (1979).

[22]M. H. Macfarlane and S. C. Peiper, Argonne National Laboratory Report No. ANL-76-11, Rev. 1, 1978 (unpublished); M. Rhoades-Brown, M. H. Macfarlane, and S. C. Peiper, Phys. Rev. C **21**, 2417 (1980); **21**, 2436 (1980).

[23]J. Lisantti, F. E. Bertrand, D. J. Horen, B. L. Burks, C. W. Glover, D. K. McDaniels, L. W. Swenson, X. Y. Chen, O. Haüsser, and K. Hicks, Phys. Rev. C **37**, 2408 (1988).

[24]M. J. Martin, Nucl. Data Sheets **47**, 797 (1986).

[25]S. J. Seestrom-Morris, C. L. Morris, J. M. Moss, T. A. Carey, D. Drake, J.-C. Dousse, L. C. Bland, and G. S. Adams, Phys. Rev. C **33**, 1847 (1986).

[26]A. M. Bernstein, V. R. Brown, and V. A. Madsen, Phys. Lett. **103B**, 255 (1981).

[27]D. Rychel, R. Gyufko, B. van Krüchten, M. Lahanas, P. Singh, and C. A. Wiedner, Z. Phys. A **326**, 455 (1987); G. J. Wagner, P. Grabmayr, and H. R. Schmidt, Phys. Lett. **113B**, 447 (1982).

[28]D. J. Horen, J. R. Beene, and F. E. Bertrand, Phys. Rev. C **37**, 888 (1988).

[29]G. R. Satchler, Nucl. Phys. **A491**, 413 (1989).

[30]G. R. Satchler, *Direct Nuclear Reactions* (Oxford University Press, Oxford, 1983).

[31]G. O. Bolme, L. S. Cardman, R. Doerfler, L. J. Koester, Jr., B. L. Miller, C. N. Papanicolas, H. Rothhaas, and S. E. Williamson, Phys. Rev. Lett. **61**, 1081 (1988).